ISSN (Print) 1226-1750
ISSN (Online) 2233-6656
Journal of Magnetics 24(2), 230-239 (2019) https://doi.org/10.4283/JMAG.2019.24.2.230

Performance Prediction and Analysis of Adjustable-speed Permanent Magnet Eddy-current Couplings

Zhao Li[1]*, Boyang Qu[1], and Dazhi Wang[2]

[1]*School of Electronic and Information Engineering, Zhongyuan University of Technology, China*
[2]*School of Information Science and Engineering, Northeastern University, China*

(Received 7 November 2017, Received in final form 28 May 2019, Accepted 30 May 2019)

This paper presents an accurate yet simple analytical model to predict the torque characteristics of an adjustable-speed permanent magnet eddy-current coupling in the low slip working area. Based on an improved magnetic equivalent circuit method, the flux density is quantitatively calculated, and then the general explicit expression of electromagnetic torque is developed. Moreover, the saturation effect of ferromagnetic materials and the restricted slip have been reasonably taken into account. Compared with the 3-D finite element analysis and measurement results, the validity of this model is confirmed. In addition, several important parameters of such devices are analyzed and discussed.

Keywords : analytical model, eddy-current couplings, magnetic equivalent circuits

Nomenclature

B : Magnetic flux density [T]
H : Magnetic field intensity [A/m]
T : Torque [N·m]
Φ : Magnetic flux [Wb]
R : Reluctance
L : Length [mm]
W : Width [mm]
h : Height [mm]
μ : Permeability [H/m]
n : Rotation speed [r/min]
σ : Conductivity [S/m]
τ_p : Pole pitch [m]
ω : Angular speed [rad/s]
v : Translational speed [m/s]
s : Slip speed
p : Pole-pairs.

Subscripts

av : Average
g : Air gap
m : Magnet
pe : Peak value
p, s : Primary and secondary sides
cs : Copper sheet
id, od : Inner and outer diameters
yp, ys : Primary and secondary yokes

*Corresponding author: Tel: +86 15524087650
Fax: +86-0374-3216995, e-mail: lz.b.y@163.com

1. Introduction

As the novel torque-transfer and speed-regulating devices, permanent magnet eddy-current couplings (PMECC) are attracting more and more attention. Compared with the existing counterparts, such as variable-frequency drives and valves, they have some distinct advantages, such as soft starting, and damping the shocks and vibrations [1, 2]. In general, the load speed can be controlled mechanically by adjusting the air-gap length between the magnet rotor and conductor rotor.

In the past decades, numerical and analytical methods have been widely used in the design and analysis of such devices [3-12]. Finite element analysis (FEA), as an important numerical approach, mostly employed in a form of package, is approbated by enterprises and research institutions. Although mature and powerful, this method is computationally intense and lack of flexibility and inclusiveness in the optimal design of machines. Thus, in most cases, FEA is used to verify and analyze the performance of an available or candidate design.

Analytical method, trading a better calculation speed

for the accuracy, is one of the most active research fields in PMECC, for example, 2-D analytical model in [6-11], and 3-D model in [12-15]. In general, most of the analytical expressions are obtained by solving Laplace and Poison's equations based on the separation variable method. In addition, many assumptions are always adopted in these models, for instance a constant conductivity in conductor region and infinite permeability and zero conductivity in iron region. All above limit the application of this method in design optimization of PMECC.

Magnetic equivalent circuit (MEC) is one of the oldest techniques for solving magnetic field problems. The approach has been applied in all sorts of electromagnetic machines, for example, permanent-magnet motor in [16-19], brushless doubly fed reluctance generator in [22] and induction machines in [20, 21]. Due to the similarity in form between magnetic circuit and electric circuit, it is easy to facilitate understanding. MEC is a compromise of the aforementioned methods, offering some benefits, such as less computational complexity and satisfactory accuracy. Some previous work on the application of MEC in such devices is given in [23-25]. However, in our work, sub-region MEC is developed, which can considerably reduce the complexity of the model and analysis.

The aim of this paper is to develop an efficient and accurate method for the analysis and design of PMECC in the low slip working area. To this end, an improved MEC method is proposed. In addition, the application condition of the model and the parameters setting are also discussed. In the end, 3-D nonlinear FEA and prototype test are applied to validate the model.

2. Analytical Model

2.1. Configuration and description

The topology of PMECC is shown in Fig. 1a. Its main body consists of two parts: one is PM rotor with axially magnetized PMs and connected to the prime mover; the other is conductor rotor and connected to the load. Two back yokes are used to close the flux and improve the magnetic circuits; an aluminum plate is used to mechanically protect the PMs. An actuator is added to adjust the air-gap, and then the output speed can be changed.

To simplify the analysis, the structure is cut in a radial direction and circumferentially expanded along with the average radius $L_{av} = (L_{id} + L_{od})/2$. Fig. 1b shows the simplified two-dimensional model and geometrical parameters, where the x-axis, y-axis, z-axis indicate the tangential direction, the axial direction, and the radial direction, respectively. Considering the symmetry of geometry and the periodicity of the magnetic field, the magnetic circuit with a pair of poles is analyzed, as shown in Fig. 1b, the black arrows display the main flux path. Table 1 presents the dimensions and the materials properties of the studied device.

Table 1. Dimensions and materials properties.

Symbols	Parameters	Values
L_m	Length of magnets	30 mm
W_m	Weight of magnets	20 mm
h_m	Height of magnets	30 mm
p	Pole-pairs number	9
L_g	Length of air-gap	variable
h_{cs}	Height of copper sheet	10 mm
L_{id}	Inner radius of copper sheet	140 mm
L_{od}	Outer radius of copper sheet	90 mm
h_{yp}	Height of primary iron yoke	20 mm
h_{ys}	Height of secondary iron yoke	20 mm
B_r	Remanence of magnets	1.27 T
H_c	Coercivity of magnets	-980 kA/m
σ_{cs}	Conductivity of copper	58 MS/m
μ_0	Vacuum permeability	$4\pi \times 10^{-7}$ Wb/(A·m)

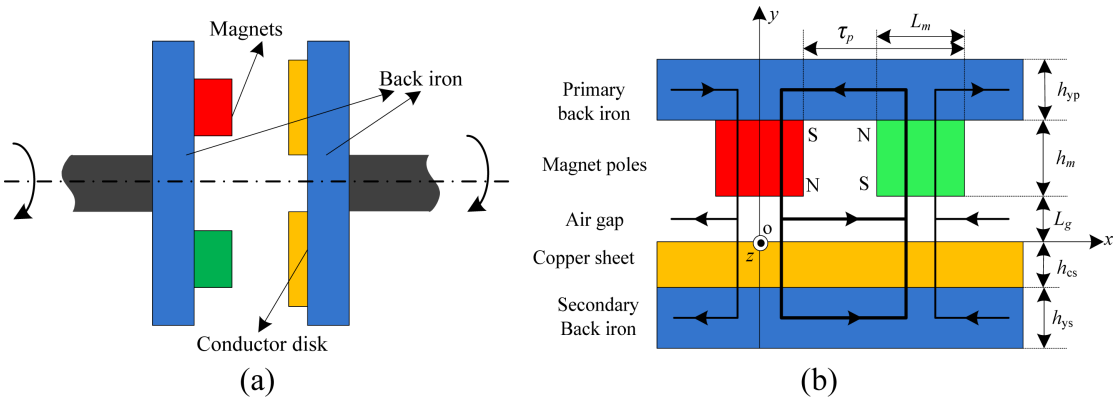

Fig. 1. (Color online) Geometry of the studied PMECC: (a) Overall structure of axial-flux PMECC (b) 2-D layer model and flux paths.

2.2. Decoupling thought of magnetic circuit

In the analysis of electromagnetic devices, employing the conventional MEC, each PM block is used as an integral magnetic source. That will produce a giant and complicated magnetic network, where the branches are coupled with each other. Assume that each branch of MECs is separated by dividing the magnetic sources and the magnetic circuits, the field analysis will be greatly simplified; and the intriguing sub-MEC can be free for analysis and study without being affected by the others. In particular, the above process is regarded as the decoupling of the MECs.

A well-known fact is that flux lines constitute the closed path from the north to the south and never intersect with each other. Fig. 2 shows the 2-D magnetic flux distribution of the studied topology. Take it for example, if the flux lines are divided into different regions, each region cannot possibly overlap with another. Moreover, it can be seen the leakage flux only exhibits at the edge of PMs. In case the MECs are divided into inner-region MEC (IRMEC) and outer-region MEC (ORMEC), every sub-region MEC has independent flux source and loop. If this division is appropriate, such as the inner region is narrow, the leakage flux will only appears in the ORMEC and the IRMEC will be ideal. And then the IRMEC can be solved in a form of simple circuit, while the ORMEC will be divided further into more sub-region MECs until all the sub-region MECs are independent.

2.3. Initial decoupling of magnetic circuit

Based on the above idea, the flux source is firstly divided into two sub-regions. The resulting sub-region MECs of initial decoupling are shown in Fig. 3. As shown, ORMEC and IRMEC are independent, and overall magnetic equivalent circuits get simple and distinct. In Fig. 3, Φ_{mi} and Φ_{mo} are the flux sources of IRMEC and ORMEC, respectively; R_{mi} and R_{mo} are the corresponding internal reluctances, respectively; R_{gi} and R_{go} are the air-gap reluctances in the two sub-region MECs; R_{sy1} and R_{sy2} are different reluctances in the secondary back iron; R_{py1} and R_{py2} are different reluctances in the primary back iron; and R_{pl} is the leakage reluctance in the ORMEC.

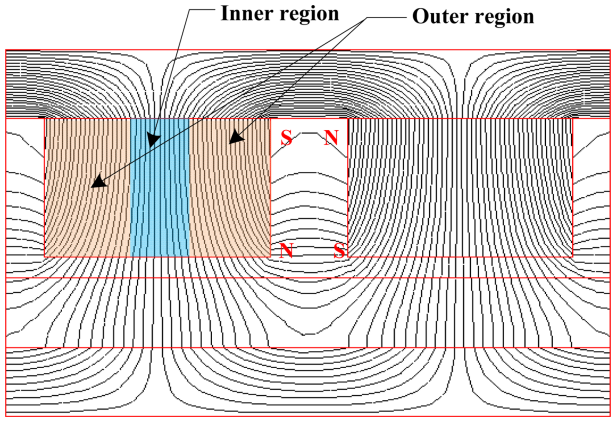

Fig. 2. (Color online) 2-D magnetic flux distribution.

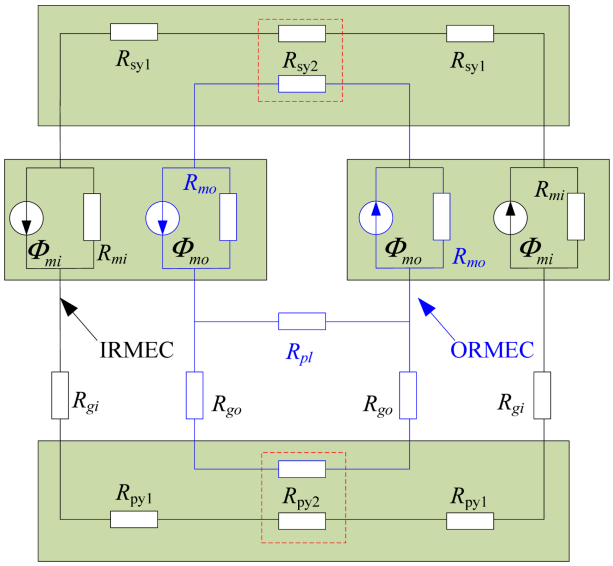

Fig. 3. (Color online) Sub-region magnetic equivalent circuits of initial decoupling.

Fig. 4 shows the independent IRMEC and its simplified schematic. Assume that the ideal inner-region magnetic circuit width is t. By definition, the flux source of IRMEC and the internal reluctance can be expressed as follows

$$\Phi_{mi} = 0.5tB_rW_m \tag{1}$$

$$R_{mi} = \frac{h_m}{t\mu_0\mu_rW_m}, \mu_r = -\frac{B_r}{\mu_0H_c} \tag{2}$$

The total air-gap reluctance of IRMEC can be calculated as follows

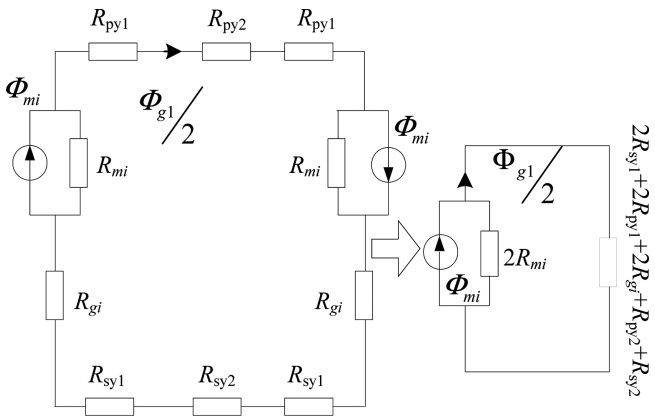

Fig. 4. IRMEC and simplified schematic.

$$R_{gi} = \frac{2(g + h_{cs})}{t\mu_0 W_m} \tag{3}$$

The reluctances of the back iron are divided into three sections [22]. Based on the general calculation formula of reluctance, the following expression can be obtained

$$R_{sy1} = \frac{0.5t}{\mu_{sy}\mu_0(A_1 + A_2)/2},\ R_{sy2} = \frac{\tau_p - t}{\mu_{sy}\mu_0 A_1/2} \tag{4}$$

where,

$$A_1 = H_s L_m,\quad A_2 = 0.5tW_m \tag{5}$$

In the same way, the reluctances of the primary back iron can be calculated as follows

$$R_{py1} = \frac{0.5t}{\mu_{py}\mu_0(h_{py}L_m + 0.5tW_m)/2},\ R_{py2} = \frac{\tau_p - t}{\mu_{py}\mu_0 \frac{h_{py}}{2} L_m} \tag{6}$$

where, μ_{py} and μ_{sy} are the relative permeabilities of the associated steel yokes. Considering the saturation effect of ferromagnetic material, they should be cautiously chosen. To determine the appropriate relative permeability of iron material, a simple and effective average equivalent permeability method is adopted [26].

According to the simplified MEC model shown in Fig. 4 and the fundamental theory of electromagnetism, the magnetic flux and magnetic flux density of the middle air-gap in IRMEC can be deduced as follows

$$\Phi_{g1} = \frac{4R_{mi}}{2(R_{py1} + R_{sy1} + R_{gi} + R_{mi}) + R_{py2} + R_{sy2}} \cdot \Phi_{mi} \tag{7}$$

$$B_{g1} = \frac{\Phi_{g1}}{tW_m} \tag{8}$$

2.4. Secondary decoupling of magnetic circuit

It's evident that the ORMEC is not a simple MEC model, which contains the leakage magnetic circuits. Based on the decoupling thought of magnetic circuit, the complicated ORMEC in Fig. 3 is further divided into different sub-region MECs. To facilitate implementation and get more accurate results, some assumptions should be made as follows

1) All the magnetic flux lines are uniformly distributed and pass through the permanent magnets vertically without leakage.

2) Leakage magnetic circuits from the air-gap and the inter-pole emerge.

3) Considering the brow leakage is the main leakage flux, which mainly exists near the ends of the magnets, the width of leakage flux source should be smaller than half of the PM thickness. Otherwise, the leakage magnetic field will be stronger than the air-gap magnetic field.

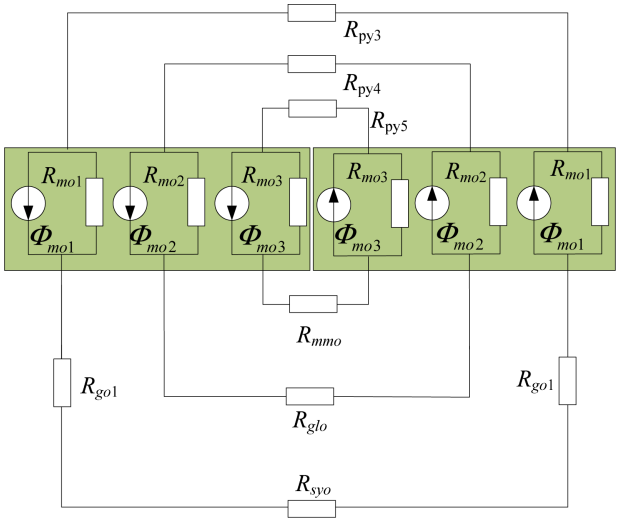

Fig. 5. (Color online) Decoupling of outer-region magnetic equivalent circuit.

The ORMEC is composed of three sub-MECs shown in Fig. 5. As can be seen from Fig. 5, air-gap loop, air-gap leakage flux loop and N-pole to S-pole leakage flux loop are distinct, and completely decoupled. In Fig. 5, Φ_{mo1}, Φ_{mo2} and Φ_{mo3} are the flux sources, which correspond to air-gap loop, air-gap leakage flux loop and N-pole to S-pole leakage flux loop, respectively; R_{mo1}, R_{mo2} and R_{mo3} are the internal reluctances of the three flux sources, respectively; R_{go1} is the total reluctance in the air-gap and conductor plate of air-gap loop; R_{glo} is the total reluctance in the air-gap and conductor plate of air-gap leakage flux loop; R_{mmo} is the gap reluctance of N-pole to S-pole leakage flux loop; R_{py3}, R_{py4} and R_{py5} are the reluctances in the primary steel-yoke; R_{syo} is the reluctance of the secondary steel-yoke.

The coordinate system in Fig. 1b is employed. Considering the magnetic flux density in the air-gap decrease along the x-direction in [0, $\tau_p/2$], for simplicity and quantitative analysis, the magnetic flux density in the air-gap of ORMEC is assumed a quadratic curve, which can be written as

$$B_{g2}(x) = a_0 x^2 + a_1 x + a_2 \tag{9}$$

where, a_0, a_1 and a_2 are unknown constants to be determined, and can be obtained by the following conditions

1) The flux lines in the air-gap are as many as those traversing through the magnet poles.

2) In the boundary of different sub-region MECs, the magnetic flux density should be identical.

3) As the magnetic field distributes symmetrically, the

magnetic flux density should be zero in the middle of the two adjacent magnet poles.

The foregoing analysis can be exhibited by means of analytical expressions as follows

$$\int_0^{\frac{\tau_p - t}{2}} B_{g2}(x) W_m dx = B_{g1} W_m \left(\frac{L_m - t}{2} - l_0 \right) \tag{10}$$

$$B_{g2}(x)\Big|_{x=\frac{1}{2}t} = B_{g1} \tag{11}$$

$$B_{g2}(x)\Big|_{x=\frac{\tau_p}{2}} = 0 \tag{12}$$

where l_0 is the width of flux leakage source in ORMEC shown in Fig. 5.

Within the scope of one pole pitch, in the static state, the axial flux density in the air-gap is as follows

$$B_g = \begin{cases} B_{g0}, & x \in [-\dfrac{L_m + \tau_p}{2}, -t/2) \\ B_{g1}, & x \in [-t/2, t/2] \\ B_{g2}, & x \in (t/2, \dfrac{L_m + \tau_p}{2}] \end{cases} \tag{13}$$

where B_{g0} and B_{g2} are completely symmetric about the y-axis, thus $B_{g0} = a_0x^2 - a_1x + a_2$.

3. Torque Model

3.1. Transmission torque

Research has shown the efficiency of eddy-current couplings is optimal in the case of low slip [7, 10], thus, it makes more sense to study the torque model in this condition. Moreover, in such case, the reaction field produced by the eddy currents in conductor plate can be ignored [10, 24], therefore, the effective magnetic field in the air-gap is approximatively derived from PM, i.e. B_g. According to the working principle of eddy-current drivers, the transmission torque in magnitude is equal to the braking torque. And this is mainly produced by induced current losses dissipated in the conductive plate. The eddy currents induced in the conductive plate can be calculated from Lorentz's equation,

$$J = \sigma_{cs} v \times B = \sigma_{cs} L_{av} B_g \tag{14}$$

Thus, the eddy current loss can be given as follows

$$P = W_m \sigma_{cs}^{-1} \iint_{cs} |J(x)|^2 dxdy \tag{15}$$

and the transmission torque is given by

$$T = P / \omega = W_m / \sigma_{cs} \omega \iint_{cs} |J_{cs}(x)|^2 dxdy \tag{16}$$

where, $\omega = \omega_p - \omega_s$. Substituting (14) into (16) yields

$$\begin{aligned} T = 2pH_{cs} W_m R_{av}^2 \sigma\omega \Bigg\{ & \frac{2}{5} a_0^2 \left[\left(\frac{\tau_p}{2} \right)^5 - \left(\frac{t}{2} \right)^5 \right] + \\ & a_0 a_1 \left[\left(\frac{\tau_p}{2} \right)^4 - \left(\frac{t}{2} \right)^4 \right] + 2a_1 a_2 \left[\left(\frac{\tau_p}{2} \right)^2 - \left(\frac{t}{2} \right)^2 \right] + \\ & \left(\frac{4}{3} a_0 a_2 + \frac{2}{3} a_1^2 \right) \left[\left(\frac{\tau_p}{2} \right)^3 - \left(\frac{t}{2} \right)^3 \right] + a_2^2 (\tau_p - t) + B_{g1}^2 t \Bigg\} \end{aligned} \tag{17}$$

3.2. Consideration of 3-D effects

Although (17) can be used to evaluate transmission torque characteristics, the results in magnitude have wide deviation. Consider the solution of eddy-current is by nature a 3-D problem, as previously described, to simplify the analysis, it is reduced to 2-D model, which causes the 3-D effects of eddy-current to be ignored. However, the

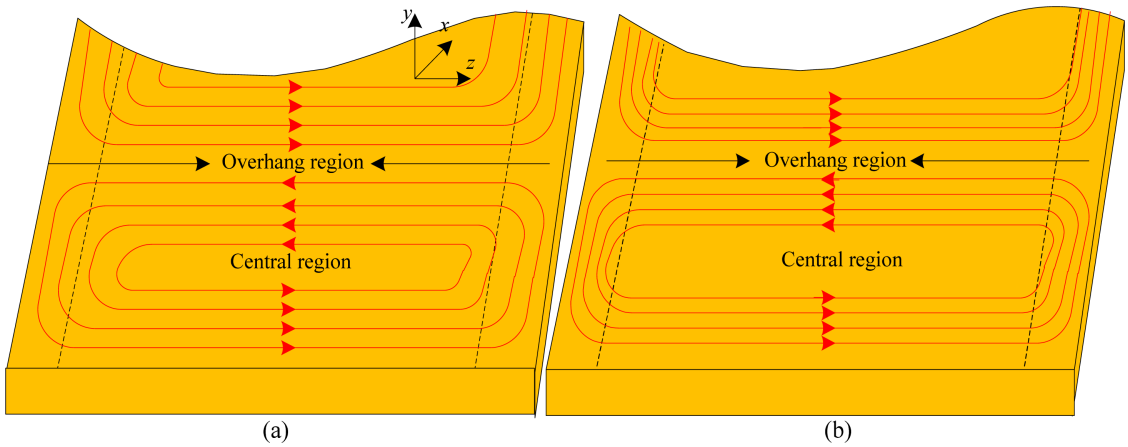

Fig. 6. (Color online) Eddy current paths in the case of: (a) low slip speed, and (b) high slip speed.

induced currents not only flow in the *z*-direction, but also *x*-direction, as shown in Fig. 6(a). There is no doubt the *x*-direction currents make no contribution to transmission torque, yet produce joule loss. Among the numerous correction methods, Russell and Norsworthy factor [27] is most popular and recognized, and has been widely adopted in electromagnetic devices. Herein, the correction factor is given by

$$k_c = 1 - \frac{\tanh\frac{\pi W_m}{2\tau_p}}{\frac{\pi W_m}{2\tau_p}[1+\tanh\frac{\pi W_m}{2\tau_p}\times\tanh\frac{\pi(L_{\mathrm{od}}-L_{\mathrm{id}}-W_m)}{2\tau_p}]} \quad (18)$$

Thus, the transmission torque of axial-flux permanent magnet eddy-current couplings can be expressed as follows

$$T_o = k_c T \quad (19)$$

3.3. Consideration of restricted slip

In the case of high slip, the eddy current paths are shown in Fig. 6(b), which are significantly different from the case of low slip shown in Fig. 6(a) and gather in a small region. Thus, the derivation conditions of Russell-Norsworthy factor are broken. In other words, the correction factor k_c is valid only in a certain slip range. It is necessary to quantitatively give the restricted slip of (19), which is helpful and instructive to the designers and engineers. Thus, the corresponding restricted slip speed has to be deduced. J.H. Wouterse in [28] studied the critical torque and speed of brake with circular magnets. In view of the similarity of the structures and operation principles, some conclusions of eddy-current brake are valid for axial-flux PM eddy-current couplings.

The critical slip speed of eddy-current brake with circular magnets can be given by

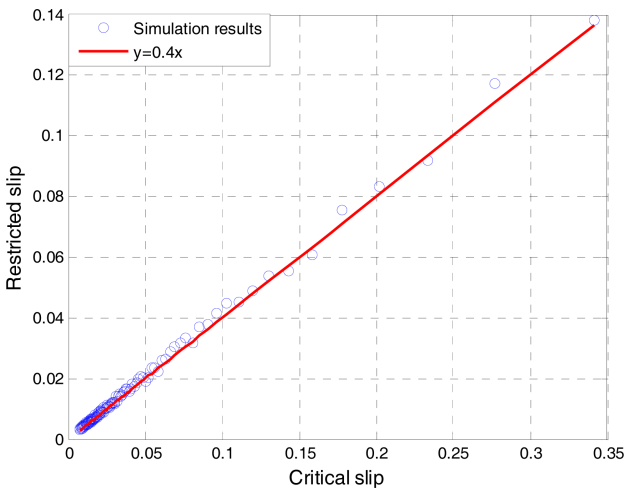

Fig. 7. (Color online) Relationship between the restricted slip and the critical slip.

$$v_k = \frac{2}{\mu_0\sigma h_{\mathrm{cs}}}\sqrt{\frac{1}{\varsigma d}}\sqrt{\frac{L_g + h_{\mathrm{cs}}}{Z}} \quad (20)$$

where, ς is an unknown proportionality factor and set to 1, which has little effect on the results. And

$$d = 2\sqrt{L_m W_m / \pi} \quad (21)$$

$$Z = \frac{1}{2}[1 - \frac{\pi^2}{24}(\frac{d}{L_{\mathrm{od}} - L_{\mathrm{id}}})^2] \quad (22)$$

and Z is the ratio of total contour resistance to resistance of contour part under magnet poles; d is the equivalent diameter, which can be expressed by the same availability magnetic area between circular magnet and other shapes of magnets.

Taking into account the speed and slip to meet the

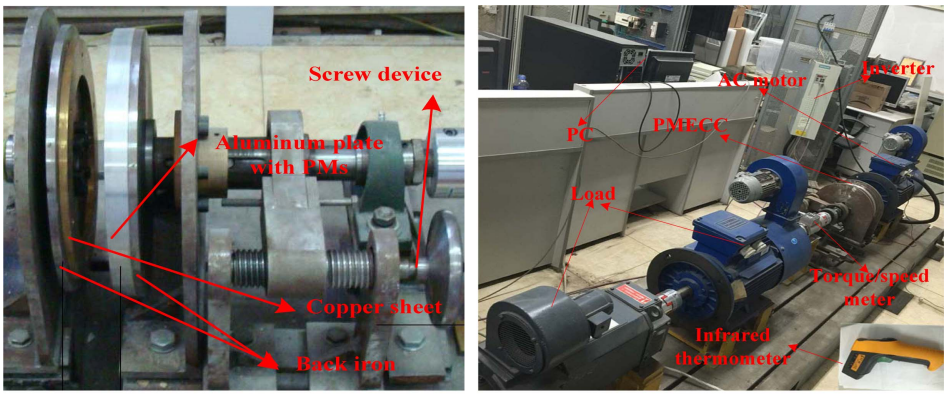

(a) (b)

Fig. 8. (Color online) Physical prototype and test platform: (a) Physical prototype and its structure (b) Test platform system and its composition.

relationship [9],

$$v = \frac{2\pi p n_1 s \tau_p}{60} \tag{23}$$

Thus, the critical slip can be given by

$$s_c = \frac{60}{p\mu_0 \sigma H_c \tau_p n_p} \sqrt{\frac{g + h_{cs}}{Zd}} \tag{24}$$

In fact, it is difficult to deduce theoretically the restricted slip. Thus, it has to be determined to follow the principle that it has minimal departure from the analytical solution. Fig. 8 shows the relationship between the restricted slip and the critical slip when the maximum error of the proposed model is 10 %, employing 3-D FEM simulation. It can be easily found that the restricted slip is a distribution of s_c. When almost all cases are satisfied, the restricted slip can be expressed as

$$s_r = \beta s_c \tag{25}$$

herein, β is 0.4 in this study.

4. Valuation and Discussion

According to the geometric parameters listed in Table 1, a prototype is manufactured, which is shown in Fig. 9a, and a screw device is added to adjust the air-gap length to control the output torque. In addition, Fig. 9b shows the constitution of the test system. The details related to experiment are as follows:

(1) The AC motor controlled by the inverter is connected with the input of PMECC, and the DC motor controlled by the governor connected with the output of PMECC as the load. In addition, the torque/speed meter is used to measure the output speed and torque.

(2) In order to test the torque-speed characteristic, the air-gap length is fixed at 3 mm, and the output speed of prime mover is adjusted by the inverter to generate

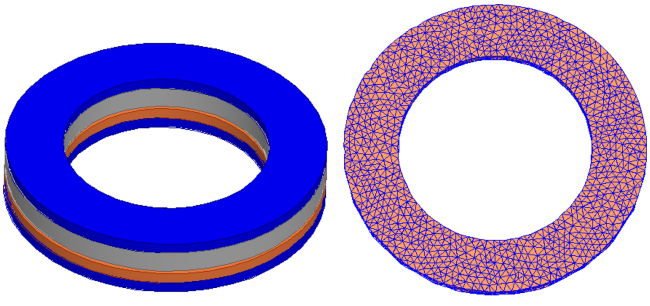

(a) (b)

Fig. 9. (Color online) 3D-FEM: (a) Model and (b) meshing of copper plate.

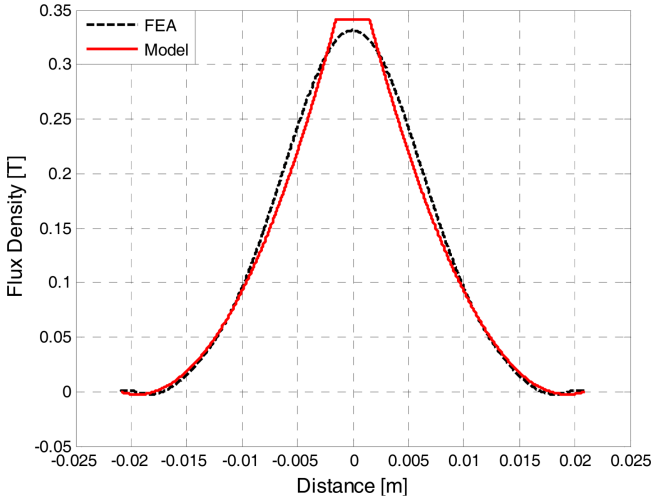

Fig. 10. (Color online) Air-gap flux density distribution in at L_g = 3 mm.

different slip speed, thereby gain different output torque.

(3) In order to test the effect of air-gap length, the output speed of prime mover is fixed at 1455 r/min, and the air-gap length can be changed by adjusting the screw device.

(4) Before star-tup, the air-gap length is adjusted to be the maximum; after that, it is adjusted to be the right value. And the infrared thermometer is used to monitor the temperature of copper sheet.

The 3-D FEA, in the software package form of ANSOFT Maxwell (ANSYS, 16.0), is employed as a benchmark. The used 3D model and meshing of conductor plate are shown in Fig. 10. Apparently the 3-D model has taken into account the existing edge effects, which are fully ignored in the analytical model. The details related to FEA are as follows:

(1) A desktop PC (32 G (RAM) with 8 cores) is employed. To ensure the analysis accuracy, the FEA model is established according to the actual size shown in Table 1.

(2) Considering the leakage flux, an air mask is added to cover the FEA model. The internal space is the solution area, and the outer space can be considered a zero equal magnetic surface.

(3) The solver type is the transient magnetic; the excitation source is the eddy current of conductor plate; the conductor plate and its yoke are used to assign band, and slip velocity is used as the motion angular velocity; a motion angular of π is concerned; a fine mesh is assigned for the conductor plate, and other parts are assigned the default mesh.

4.1. Model validation

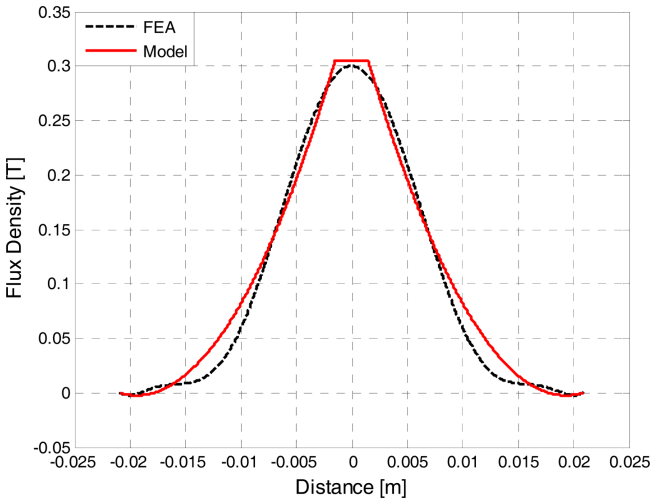

Fig. 11. (Color online) Air-gap flux density distribution at L_g = 8 mm.

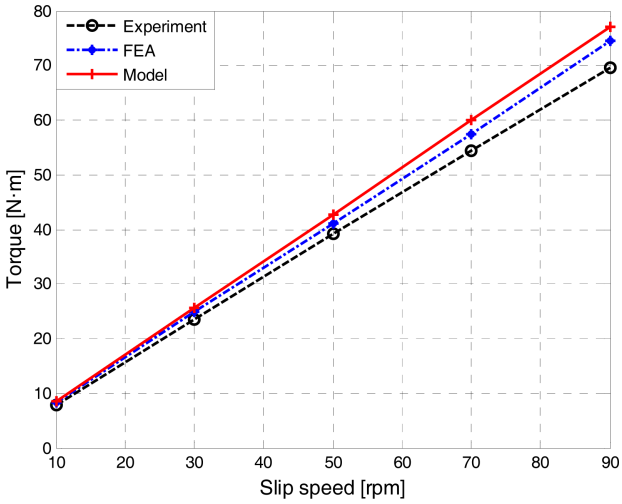

Fig. 12. (Color online) Torque-speed characteristic curve.

Fig. 11 and Fig. 12 illustrate the flux density distribution in the air-gap at L_g = 3 mm and 8 mm, respectively. It should be noted that the value of t is set to 3 mm, and l_0 is set to 6 mm in this study. A pole pitch length is considered. As shown, the predicted results are very close to those obtained by the finite element analysis, especially in the case of a small air-gap length.

Fig. 13 shows the torque-speed characteristic of PMECC, where the results obtained by FEA, measurement and analytical model are compared. As shown in Fig. 13, a value of L_g = 3 mm and a slip speed of 50 r/min are considered. It can be observed that the analytical predictions are in good agreement with the experiment and FEA. As previously mentioned, the model can give accurate predictions in the case of low slip, moreover, the maximum deviation never exceeds 10 %. In addition, it

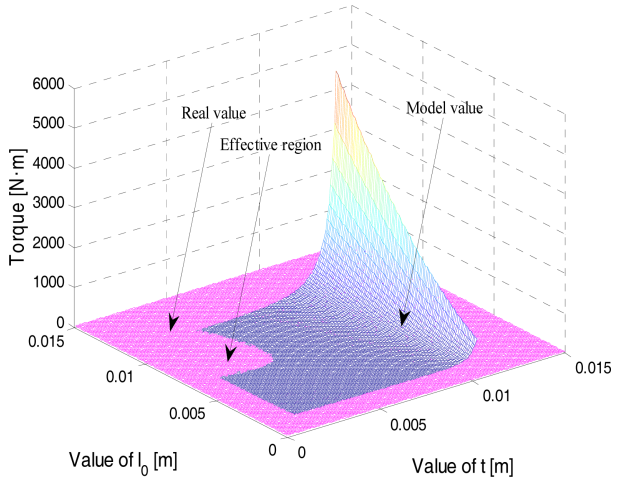

Fig. 13. (Color online) Torque versus t and l_0 at 50 r/min for L_g = 3 mm.

also shows that, with the increase of the slip, the deviation will get worse.

According to (25), the restricted slip speed is approximately given. Table 2 shows a comparison of average error rate, working in the regions with less than s_r and greater than s_r. It can be noticed that in the regions with greater than s_r, the average error rates of the analytical model are very large, and all above 20 %, but in the opposite regions, the average error rates are acceptable. Although the value of s_r might be not very accurate, it still gives a helpful guidance for the use of such devices and the proposed analytical model.

As a matter of fact, the deviation can be further analyzed by using the electromagnetic theory. When the devices work under the normal working range area, which corresponds to the low slip values, the resulting reaction field, due to the induced current, is relatively small. In this condition, the torque is proportional to the slip [21]. However, with the increase of the slip values, the resulting reaction field will not be able to ignore, and tends to distort the original flux distribution produced by the PM, and thus the effective air-gas magnetic field will be the sum of the PM field and the reaction field [3, 16, 23]. In this condition, the derivation of the torque becomes complicated and (19) will no longer be accurate, but the

Table 2. Error rates in different regions.

Air-gap length (mm)	Error rate (%)	
	$\leq s_r$	$> s_r$
3	4.5	21.3
6	5.1	25.1
9	5.8	28.8

proposed method can be potentially combined with other method developed in [16, 23] to get good results.

4.2. Analysis of model parameters

In the proposed prediction model, t and l_0 are two very important parameters. Further investigations show that they directly affect the accuracy of the prediction results. In this section, the influences and selection mechanism of t and l_0 are investigated. For the sake of simplifying analysis, the air-gap and slip speed are fixed at 3 mm and 50 r/min, respectively.

Fig. 13 shows the variation of the transmission torque with t and l_0. The real value of transmission torque under such condition is experimentally 40 N·m. As shown, when unreasonable t and l_0 are used, the magnitude of the error will be very large, causing the model to be invalid. Moreover, the effective range of t and l_0 is very small, in other words, the proposed model is very sensitive to t and l_0. A lot of analysis and emulation suggest that the prediction results of such model are acceptable when t and l_0 are around 1/10 and 1/5 of the circumferential length of PM, respectively. These will provide a criterion for the parameters selection when the method is used.

Table 3. Magnetic properties of all materials.

Component	Material	Relative permeability
PM	Nd-Fe-B: N38H	1
Coductor plate	Brass: H62	1
Back iron	Steel: 45#	Nonlinear calculation
Aluminum plate	6010#	1

Table 4. Torque variations with structure parameters.

Structure parameters	Variation	FEM (N.m)	Analytical (N.m)
Height of PM	20 mm	30.0	31.9
	25 mm	35.8	37.8
	30 mm	41.0	42.8
	35 mm	45.2	46.9
	40 mm	48.5	50.5
Pole-pairs	6	22.9	22.0
	7	26.8	28.3
	8	33.7	35.2
	9	41.3	42.8
	10	49.5	51.2
Thickness of conductor plate	6 mm	29.9	31.5
	8 mm	35.8	37.8
	10 mm	40.7	42.8
	12 mm	44.9	46.7
	14 mm	47.8	49.7

4.3. Analysis of structure parameters

The prediction model is usually used to study the effects of structure parameters in the initial design stage. In this section, three important parameters, namely, height of magnets, thickness of copper sheet as well as pole-pairs number are concerned. Table 4 shows the torque variations with these structure parameters. The air-gap and slip speed are fixed at 3 mm and 50 r/min, respectively, and the other parameters are given in Table 1. It can be observed that the torque increases with the increase of height of magnets, however, considering the growth rate is decreasing, there will be certainly an optimal value; in addition, the transmission torque will increase in a certain range of pole-pairs number, but not infinitely, once the ferromagnetic material saturates, increasing pole-pairs number cannot help the upgrade of the transmission torque, and the actual cost and volume also limit the number of permanent magnets; the transmission torque also takes on an increasing tendency with the increase of the thickness of copper sheet, and its increasing rate shows there will be an optimal thickness of copper sheet.

Moreover, the analytical results agree well with those obtained from the 3-D FEM, but the slight deviations always exist. One reason is that some leakage flux is ignored when calculating the flux density in air-gap, thus the results of proposed method will be on the large side, moreover, with the increase of air-gap length, this phenomenon is more pronounced. Another reason is that the trace of reaction flux density produced by the induced currents in conductor sheet may weaken the air-gap magnetic field produced by PM. The third reason is the 3-D geometry effects, although correction factor is introduced to counter this effect, slight differences still exist and increase with the increase of the slip speed.

4.4. Discussion of application perspective

Due to the speed control function, in some cases, for example, mines, power plants and petrochemical, etc, PMECC will gradually replace conventional transmission and hydraulic coupler, even frequency converter. Because of the non-mechanical contact, it can provide the overload protection for the generator system, and increase the lifetime of generators and motors, thus it will be applied in electric machine driven system more and more extensively. In addition, the technical principle of PMECC will be widely introduced into the brakes, retarders, and shock absorbers to develop better devices.

5. Conclusion

In this paper, an improved equivalent magnetic circuit

method is illustrated and applied to axial-flux PMECC. The analytical models of magnetic field and transmission torque are established. Compared with FEA and measurement, the results show the proposed analytical model is effective. Moreover, some key model parameters and structural parameters are studied. It is determined that the method can be used to conveniently evaluate the performances of PMECC in their initial design stages.

Acknowledgments

The work was supported in part by the National Science Foundation of China under Grant 61673404, in part by the Central Plains Thousand People Plan of Henan Province under Grant ZYQR201810162.

References

[1] J. Kim, J. Choi, M. Koo, and S. Lee, IEEE Trans. Appl. Supercond. **26**, 1 (2016).
[2] Z. Mouton and M. J. Kamper, IEEE Trans. Ind. Electron. **61**, 3367 (2014).
[3] H. Shin, J. Choi, S. Jang, and K. Lim, IEEE Trans. Magn. **49**, 3985 (2013).
[4] N. Allen, D. Rodger, P. Coles, S. Strret, and P. Leonard, IEEE Trans. Magn. **31**, 3524 (1995).
[5] S. E. Gay and M. Ehsani, IEEE Trans. Magn. **42**, 319 (2006).
[6] T. Lubin, S. Mezani, and A. Rezzoug, IEEE Trans. Energy. Convers. **27**, 536 (2012).
[7] L. Belguerras, L. Hadjout, S. Mezani, and A. Rezzoug, IEEE Trans. Appl. Supercond. **24**, 1 (2014).
[8] A. Canova and B. Vusini, IEEE Trans. Magn. **41**, 24 (2005).
[9] J. Wang, H. Lin, S. Fang, and Y. Huang, IEEE Trans. Magn. **50**, 1 (2014).
[10] T. Lubin and A. Rezzoug, IEEE Trans. Ind. Electron. **62**, 2287 (2015).
[11] Q. Lin, J. Mo, X. Dai, Y. Long, J. Cao, and S. Wang, Int. J. Appl. Electrom. **1**, 1 (2016).
[12] T. Lubin and A. Rezzoug, IEEE Trans. Magn. **51**, 1 (2015).
[13] Z. Meng, Z. Zhu, and Y. Sun, IEEE Trans. Magn. **51**, 1 (2015).
[14] R. Ravaud and G. Lemarquand, IEEE Trans. Ind. Appl. **45**, 1950 (2009).
[15] R. Ravaud, V. Lemarquand, and G. Lemarquand, IEEE Trans. Magn. **46**, 3860 (2010).
[16] S. Mohammadi and M. Mirsalim, IEEE Trans. Magn. **50**, 1 (2014).
[17] H. Yeo, D. Lim, D. Woo, J. Ro, and H. Jung, IEEE Trans. Magn. **51**, 1 (2015).
[18] B. S. Ghalavand, S. V. Zadeh, and A. H. Isfahani, IEEE Trans. Magn. **46**, 112 (2010).
[19] M. Hsieh and Y. Hsu, IEEE Trans. Ind. Electron. **9**, 779 (2012).
[20] M. Amrhein and P. T. Krein, IEEE Trans. Energy. Convers. **25**, 399 (2012).
[21] J. Qian, X. Chen, H. Chen, L. Zeng, and X. Li, Sensors **13**, 1664 (2012).
[22] M. Hsieh, I. Lin, and D. G. Dorrell, IEEE Trans. Magn. **50**, 1 (2014).
[23] S. Mohammadi, M. Mirsalim, and S. V. Zadeh, IEEE Trans. Energy. Convers. **29**, 224 (2014).
[24] M. Tsai, K. Chiou, S. Wang, and C. Lin, IEEE Trans. Magn. **50**, 1 (2014).
[25] T. Shi, D. Wang, Z. Li, and D. Zheng, Int. J. Appl. Electrom. **50**, 525 (2016).
[26] J. Wang, H. Lin, H. Li, S. Fang, Y. Huang, J. Dong, and H. Yang, IEEE Trans. Magn. **45**, 2936 (2009).
[27] R. L. Russell and K. H. Norsworthy, IEE Proc.-Part A: Power Eng. **105**, 163 (1958).
[28] J. H. Wouterse, IEE Proc.-Part B: Electron. Power Appl. **138**, 163 (1991).

Appendices

Based on the linear theory and the limiting nonlinear theory of eddy-current loss in solid iron plates, a simple and effective average equivalent permeability is proposed by Wang in [26]. The ultimate calculated formulas are as follows

$$\frac{8}{3\pi U}=\frac{1}{2\delta}\frac{\sinh 2h/\delta-\sin 2h/\delta}{\cosh 2h/\delta+\cos 2h/\delta},\ \text{for}\ U<h \tag{A.1}$$

and

$$\frac{8\times[1-\left(1-\frac{d^2}{U^2}\right)^{3/2}]}{3\pi U}=\frac{1}{2\delta}\frac{\sinh 2h/\delta-\sin 2h/\delta}{\cosh 2h/\delta+\cos 2h/\delta},\ \text{for}\ U\geq h \tag{A.2}$$

where,

$$\left.\begin{aligned}U&=\sqrt{2H_{\mathrm{pe}}/(s\omega_1 c_0 B_{\mathrm{pe}}\sigma_b)}\\ \delta&=\sqrt{2/(s\omega_1\sigma_b\mu_{\mathrm{eq}})}\end{aligned}\right\} \tag{A.3}$$

where, c_0 is the empirical coefficient and set to 0.75 [26]; σ_b is the conductivity of back iron; B_{pe} is the peak magnetic flux density of back iron; H_{pe} being the corresponding magnetic field intensity of iron characteristics, and h equals h_{py} or h_{sy}. The average equivalent permeability μ_{eq} is hidden in δ.